Conf-930899--1
BNL-48626

Powder diffraction studies using anomalous dispersion

D. E. Cox[a] and A. P. Wilkinson[b]

[a]Physics Department, Brookhaven National Laboratory, Upton, NY 11973, USA

[b]Materials Department, University of California, Santa Barbara, CA 93106, USA

Abstract

With the increasing availability and accessibility of high resolution powder diffractometers at many synchrotron radiation sources throughout the world, there is rapidly-growing interest in the exploitation of anomalous dispersion techniques for structural studies of polycrystalline materials. In conjunction with the Rietveld profile method for structure refinement, such studies are especially useful for the determination of the site distributions of two or more atoms which are near neighbors in the periodic table, or atoms which are distributed among partially occupied sites. Additionally, it is possible to i) determine the mean-square displacements associated with different kinds of atoms distributed over a single set of sites, ii) distinguish between different oxidation states and coordination geometries of a particular atom in a compound and iii) to determine f ' for a wide range of atomic species as a function of energy in the vicinity of an absorption edge.

Experimental methods for making anomalous dispersion measurements are described in some detail, including data collection strategies, data analysis and correlation problems, possible systematic errors, and the accuracy of the results. Recent work in the field is reviewed, including cation site-distribution studies (e.g. doped high T_c superconductors, ternary alloys, $FeCo_2(PO_4)_3$, $FeNi_2BO_5$), oxidation- state contrast (e.g. $YBa_2Cu_3O_{6+x}$, Eu_3O_4, $GaCl_2$, Fe_2PO_5), and the effect of coordination geometry (e.g. $Y_3Ga_5O_{12}$).

1. INTRODUCTION

In the past few years, there has been rapid progress in the development and application of high-resolution powder diffraction techniques at synchrotron sources [1,2,3]. Several beam-lines dedicated to powder diffraction are now in operation or being commissioned, and others are in the planning stages at the next-generation sources presently under construction. As in the case of dedicated neutron instruments, there is a large user community with a major interest in the determination and refinement of inorganic structures, and the study of phase transitions. In addition, the high resolution is being increasingly exploited for the *ab-initio* determination of unknown structures.

While anomalous scattering powder diffraction has been used in structural studies for many years (see, for example, the 1934 paper of Bradley and

MASTER
DISTRIBUTION OF THIS DOCUMENT IS UNLIMITED

Rodgers [4] on the distribution of Cu, Mn and Al in Heusler alloys), the success of synchrotron x-ray powder techniques has stimulated a new and growing interest in their application in this area. On a bending magnet beam-line at a 2.5 GeV machine such as the National Synchrotron Light Source (NSLS), a wide range of K- and L-absorption edges in the range 5-25 keV is accessible, which includes most of the elements between V and U. The remaining elements in this range have edges that are accessible on a wiggler beam-line or at a higher energy source.

Probably the most important application of anomalous scattering to powder diffraction is to provide contrast between neighboring elements in the periodic table, long a traditional application of neutron diffraction. This, of course, is possible because f'attains large negative values in the vicinity of the absorption edge, which markedly reduces the overall atomic scattering factor of the element in question. This can have a dramatic effect on certain classes of reflections. Furthermore, this effect is proportionally greater with increasing scattering angle, 2θ, or momentum transfer, K ($=4\pi \sin \theta/\lambda$) , since f'remains essentially unchanged as a function of these quantities. For example, at an energy 10 eV below the K-edge of Fe, theory [5,6] and experiment [7] show f'to have a value of about -6 electron units (eu), compared to 26 and 12 eu for f_0 at $(\sin\theta) / \lambda$ values of 0.0 and 0.5 $Å^{-1}$, a fairly typical range for the collection of powder data. Comparable ratios are found for heavier elements. In fact, in many cases the contrast provided by x-rays is better than that provided by neutrons.

Anomalous scattering is therefore a quite general technique for the determination of the distribution of two or more elements of similar atomic number among crystallographically distinct sites in a crystal structure. This is a very common problem in many areas of solid state chemistry and physics, metallurgy, materials science and mineralogy. In principle, the method can be applied to any number of elements, with accessible edges, in a given compound.

A related aspect is the distribution of two atomic species among partially occupied sites, which is an important feature in the chemistry of molecular sieves and microporous materials such as zeolites, for example. If one of the species has an accessible edge, details of the distribution can be obtained from two sets of diffraction measurements, one close to the edge and the other much further away. When the two species occupy a single set of sites, anomalous scattering provides a selective probe for the determination of the individual temperature factors or static displacements associated with relaxation effects [8].

A very recent application of anomalous scattering to powder diffraction has been the study of compounds in which a single element is present in two different oxidation states. This technique requires careful measurements very close to the absorption edge, since it relies in part upon the small difference in the positions of the respective edges for each oxidation state, typically a few eV, as illustrated in Figure 1. In this way, a direct assignment of each oxidation state to a specific site in the structure can be made, which is seldom possible with spectroscopic techniques. This may also be a useful method to study the behavior of an element in a single oxidation state but with different types of coordination geometry.

Anomalous scattering diffraction measurements on simple reference compounds can be used for the experimental determination of f ' as a function of energy [9,10]. Such reference materials are available for practically all elements, so this is a quite general technique. Of course, there are many other, sometimes more accurate methods that can be used for this purpose if suitable samples can be prepared, such as single crystal diffraction [11], interferometry [7], and transformation of x-ray absorption data [12,13,14]. These experimental techniques are discussed in more detail in the article by Lengeler in this book [15].

A potentially important application of anomalous scattering to powder diffraction is the estimation of phase angles as an aid to the *ab-initio* solution of unknown structures [16,17,18]. While this is a widely-used technique in macromolecular crystallography, as described in the article by Hendrickson in this book [19], it use is only just starting to be explored by the powder diffraction community.

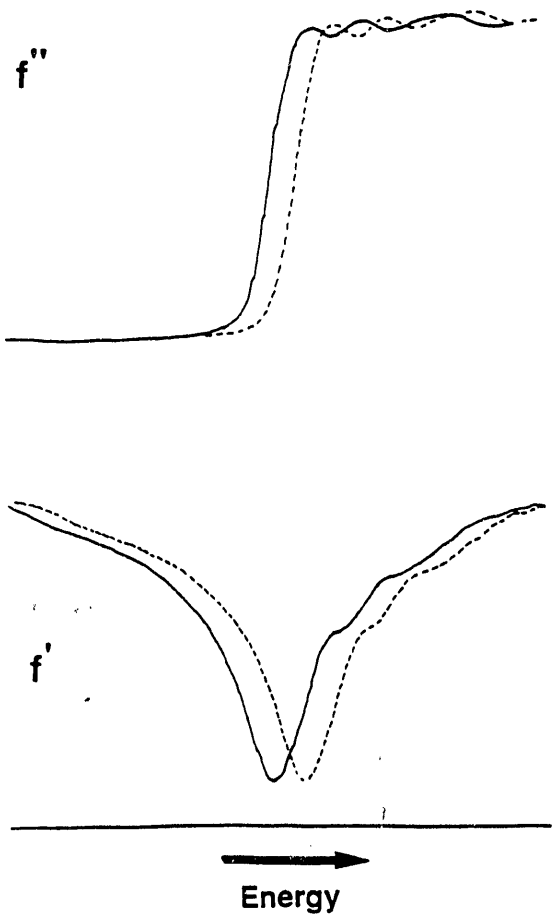

Figure 1. Schematic illustration of the shift in the curve for f ' as a function of x-ray energy from a lower (solid line) to a higher (dashed line) oxidation state. The shift is typically a few eV.

Differential anomalous scattering has proved to be a valuable technique in the study of amorphous materials [20], polycrystalline compounds showing intermediate-range order, and quasicrystals [21,22,23], and it can also be used for qualitative and quantitative analysis of minority phases in mixtures [24]. Because of space limitations these aspects cannot be considered in the current article, which is restricted to studies of long range structural features in bulk polycrystalline materials and is organized as follows. In section 2 we will outline the experimental strategy and techniques for data collection, methods for data analysis and some of the pitfalls likely to be encountered. In section 3 we will review a number of specific examples which will illustrate many of these points, and in section 4 we conclude with a few general remarks.

2. EXPERIMENTAL TECHNIQUES

2.1. Data collection strategies

Powder diffraction data collection at a synchrotron source is normally a relatively straightforward procedure compared with many other types of

experiment, but there are several important points to keep in mind in the planning stage, especially in the case of anomalous scattering investigations. A brief summary follows; more detailed accounts can be found in the recent literature [25,26,27].

It is essential to check samples on a good laboratory diffractometer for homogeneity, impurity phases, and size and strain line-broadening. The synchrotron is not the place to discover problems of this sort. Useful information about crystallite size and shape anisotropy can often be obtained from SEM micrographs. Large crystallites several microns in dimensions may make it difficult to achieve proper powder randomization, and flat-plate samples of platy or acicular materials will probably show pronounced preferred orientation effects which may be difficult to correct for in the subsequent data analysis.

The next point to consider is the choice of diffraction geometry, as illustrated in Figure 2. Typical configurations include a flat-plate or capillary sample in conjunction with a narrow receiving slit and, a scintillation counter or semiconductor detector, or a flat-plate sample with Soller slits if the beam size permits. Crystal-analyzer geometry offers the best resolution and peak-to-background discrimination, but may not give adequate counting rates, especially with narrow diameter capillary samples. Receiving-slit or Soller-slit geometry should then be considered instead. In any case, it is very desirable to make some preliminary checks of the trade-off between intensity, resolution and peak-to-background discrimination at the start of the experiment. Other possibilities include the use of a one-dimensional position-sensitive detector or an imaging plate for more rapid data collection.

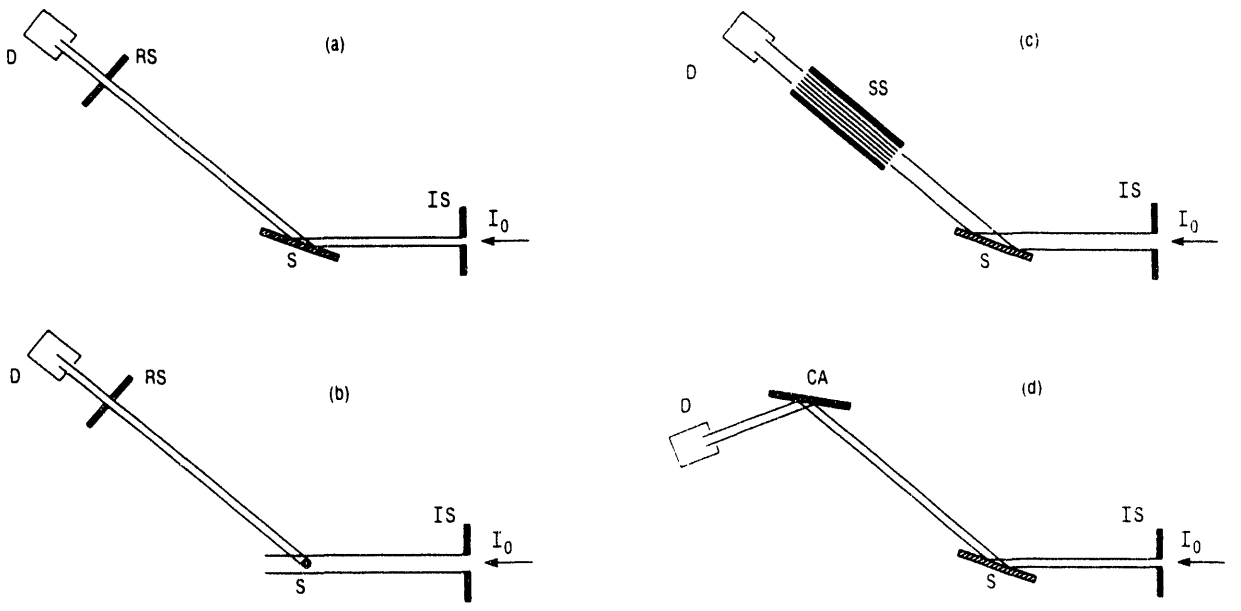

Figure 2. Various types of instrumental geometry for synchrotron x-ray powder diffraction. (a) narrow incident beam slits (IS) and receiving slit (RS), flat-plate sample (b) narrow receiving slit, capillary sample (c) Soller slits (SS), flat-plate sample (d) crystal-analyser (CA), flat-plate sample. Reproduced from ref. [3].

The energy spread in the incident beam is another important factor. This is easily estimated from the intrinsic energy resolution of the monochromator crystal, $\Delta E/E$, and the divergence of the beam in the scattering plane (usually vertical), $\Delta\varnothing$, which will depend on the source and incident beam or sample dimensions.

$$\Delta E/E = [(\Delta\varnothing \cot \theta_M)^2 + (\Delta E/E)^2_{\text{crystal}}]^{1/2} \quad (1)$$

Here θ_M is the Bragg angle of the monochromator and $(\Delta E/E)_{\text{crystal}} = \omega \cot \theta_M$, where ω is the Darwin width. For Si(111) at an energy of 10 keV, typical values of ΔE at beam-line X7A at the NSLS lie in the range 2-3 eV.

A standard procedure for preparing flat-plate samples by back-loading is described by Klug and Alexander [28]; however, since the sample must be rotated or rocked during data collection and a smooth surface is needed, it is probably best to press the sample into a recessed holder with a glass slide. This minimizes the possibility of losing part of the sample as a consequence of its motion, but unfortunately will also tend to exacerbate preferred orientation effects. If desired, such effects can usually be eliminated through the use of capillary specimens; in this case the radius of the capillary, R, should be chosen so that μR does not exceed 2, say, to avoid unduly large absorption corrections. It is a good practice to weigh the amount of material introduced and determine the effective density directly, typically 25-40%. Again, it is well worth the extra effort to carry out preliminary checks with both flat-plate samples and capillary specimens of different diameters.

If the objective of the experiment is to contrast near-neighbor elements in the periodic table and determine their distribution among different crystallographic sites, the recommended strategy is to collect two extended data sets, one slightly below the absorption edge (say 10 eV for a 3d atom), and one several hundred eV below the edge, or better still, well above the edge. It has been our experience that data collected around 0.7 Å (~18 keV) are less prone to systematic errors than those collected at the longer wavelengths which are often employed and give more reliable refinements, especially with respect to thermal parameters. In the subsequent refinement, the second data set provides a constraint which helps reduce the otherwise large correlations between thermal parameters, site occupancies, dispersion terms and the overall scale factor.

The energy difference of 10 eV for a 3d atom is chosen so that the value of f' can be estimated reliably using readily available theoretical results and to provide an adequate contrast change between the two wavelengths. The reliability of the theoretical calculations falls off rapidly close to the absorption edge due to the omission of the influence of the natural line-widths of the energy levels [29] and the instrumental energy resolution. Additionally, the chemical environment of a species also effects the anomalous scattering corrections in the near-edge region.

Since the position of the edge will depend on the oxidation state of the element in question, it is strongly recommended to determine this directly. This approach also avoids some of the difficulties associated with monochromator calibration and is easily accomplished by monitoring the $K\alpha$

fluorescence from the sample (preferably with a semiconductor detector) as the monochromator is scanned through the edge. An example of a Ga K-edge scan for $Y_3Ga_5O_{12}$ is illustrated in Figure 3 [25]. The measured edge is at about 10.377 keV compared to 10.367 keV for elemental gallium, and reflects the extra binding energy of gallium in the trivalent state. If the energy is now set to 10.367 keV, the calculated value of f ' is about -7 eu [30]. In this case the sample was the same flat-plate specimen satisfying the "infinitely-thick" criterion [28] used for the diffraction measurements, and the fluorescence curve may be somewhat distorted with respect to an absorption curve collected on a dilute sample. Nevertheless the measured edge position should be reliable enough for setting up the experiment.

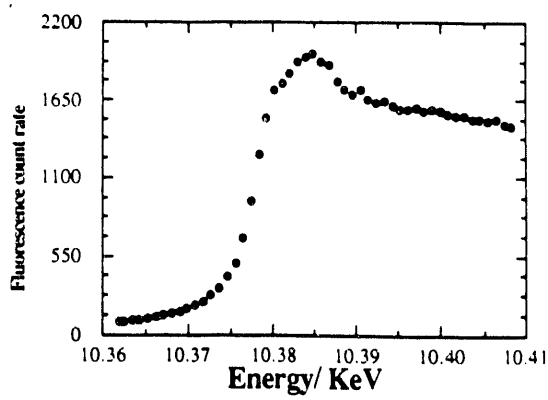

Figure 3. Fluorescence signal from a flat-plate sample of $Y_3Ga_5O_{12}$ in the vicinity of the Ga K-edge measured with a semiconductor detector. Reproduced from ref. [25].

At this stage, an accurate calibration of the energy should be carried out with a standard reference material such as Si (a = 5.4308 Å) or CeO_2 (a = 5.4113 Å). If there is some concern about the stability of the source or the beam-line optics, further calibrations may be needed to check for possible drifts in the energy.

Measurements designed to study oxidation state contrast in a compound are considerably more challenging than those involving only element contrast, since they require the accurate determination of f ' for both oxidation states in a narrow region (typically only a few eV) around the absorption edge. Good source and beam optical stability, say, to within ±1 eV, are desirable for such experiments, and calibration is necessary at frequent intervals. In the region just above the edge, counting rates and peak-to-background discrimination are vastly inferior due to the stronger absorption, as illustrated in Figure 4. Maintaining a proper powder average may also be a problem because of the decrease in the volume of material which is sampled, and systematic errors due to surface roughness effects may be greatly enhanced [31]. The advantage of using a semiconductor detector can be appreciated from the inset to Figure 4, which shows the energy spectrum obtained for a background point. By far the largest component of the scattering is the Kα fluorescence, which would increase the background by a factor of five if a conventional scintillation detector were used. In oxidation-state contrast studies of this type, valuable complementary information can be obtained from x-ray absorption spectra measured on the same sample and suitable model compounds, for example, the presence of white-line features and the likely energy difference between the respective edges can be determined. This will be illustrated in more detail by some results for $GaCl_2$ to be described in section 3.2.

The procedure for data collection is quite straightforward; step-scans are carried out at intervals appropriate to the peak widths (typically 5 or 6 points

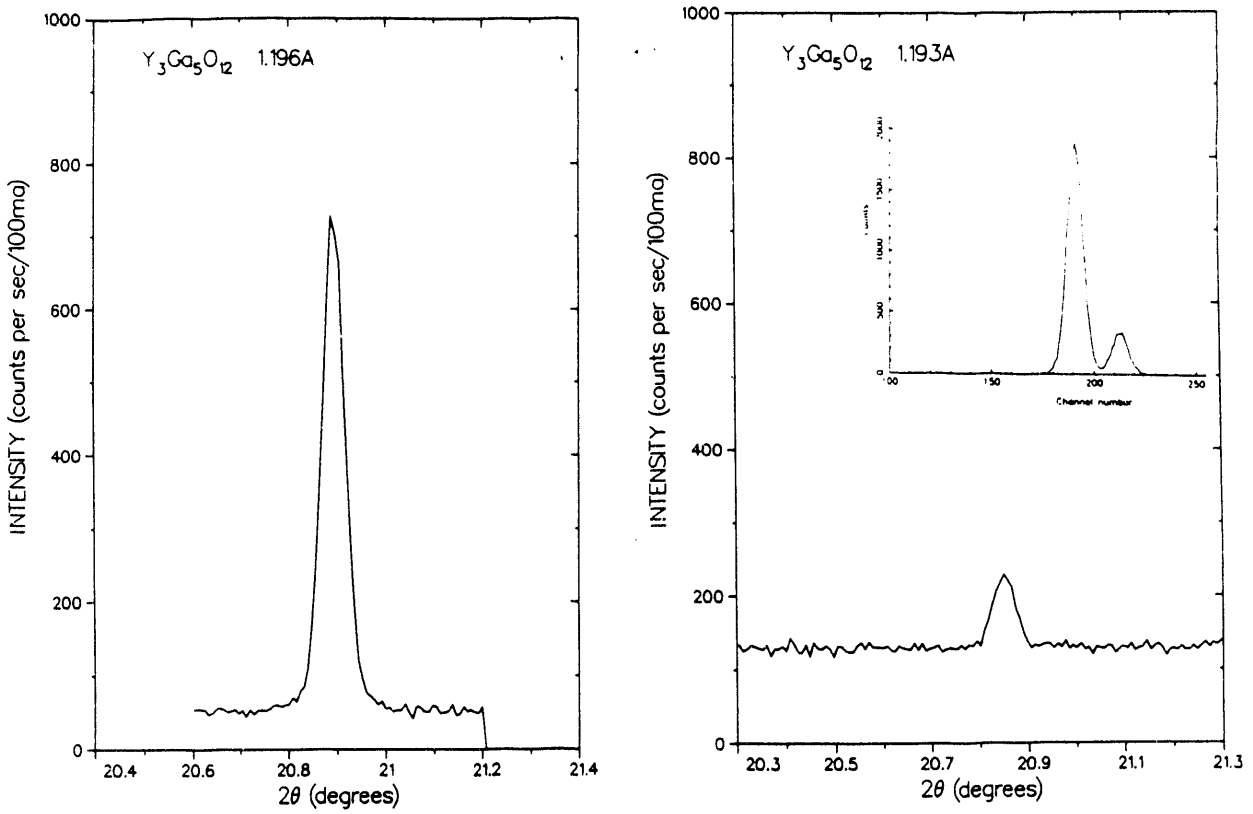

Figure 4. Scans of the (321) peak from $Y_3Ga_5O_{12}$ just below (left) and above (right) the Ga K-edge. The inset on the right shows the energy spectrum from the semiconductor detector recorded in a multichannel analyser. The strong peak is the Ga Kα fluorescence signal.

across the full-width at half-maximum) over a suitably wide angular range. For proper powder averaging it is essential to rotate or rock the sample at each point while counting. The reproducibility of the measurements should be checked by replication scans of a few strong low-index reflections.

2.2. Data analysis and structure refinement

By far the most widely used method for the analysis of powder diffraction data is the profile technique for structure refinement introduced by Rietveld in 1969 [32]. In this method, the intensity, y_i, at each point in the diffraction pattern is calculated from the expression,

$$y_i = K \sum_{k=1}^{m} F_k \, j_k \, (LP)_k \, A_i \, N \, g(\Delta 2\theta/\Gamma_k) \qquad (2)$$

where K is an instrumental scaling factor, j_k is the reflection multiplicity, $(LP)_k$ is the Lorentz-polarization factor, A_i is the transmission factor, N is a normalization constant, g is a peak shape function, $\Delta 2\theta = (2\theta_i - 2\theta_k)$ is the displacement from the peak position $2\theta_k$ and Γ_k is the peak full-width at half-maximum (FWHM). F_k is the structure factor defined in the usual way, i. e.

$$F = \sum_{j=1}^{n} (f_o + f' + if'')_j \exp[-2\pi i(hx_j + ky_j + lz_j)] \quad (3)$$

The summation in Eq. (2) is carried out over all peaks that contribute to the intensity at that point. It is important in Rietveld analysis to have a good model for the peak shape, and a variety of functions have been described in the literature, the most commonly-used one being the so-called Voigt function, which is a convolution of Gaussian and Lorentzian functions, or an approximate form first suggested by Wertheim et al. [33] and now known as the pseudo-Voigt function,

$$I \propto \eta C_L [1 + 4(\Delta 2\theta/\Gamma)^2]^{-1} + (1-\eta) C_G \exp[-4\ln 2(\Delta 2\theta/\Gamma)^2] \quad (4)$$

where C_L and C_G are normalization factors and η is the mixing parameter. The Gaussian and Lorentzian FWHM's are usually assumed to take the form,

$$\Gamma_G = (U\tan^2\theta + V\tan\theta + W)^{1/2} \quad (5)$$

$$\Gamma_L = X\tan\theta + Y/\cos\theta \quad (6)$$

These expressions allow for both instrumental resolution and for isotropic strain and particle-size broadening effects, with U, V, W, X and Y as parameters which can be varied in the refinement as desired. Each peak is assumed to contribute to the observed intensity over some range, based on either an angular range related to the peak widths or a minimum threshold intensity (say 0.1% of the peak maximum). An angular range of 5 - 10 Γ is usually taken for synchrotron X-ray peaks, since these are generally predominantly Lorentzian in character and hence have long tails. The background can be approximated by, perhaps, a Fourier series or a polynomial function; alternatively it can be estimated by interpolation between average values in regions well away from the peaks.

In general a pseudo-Voigt function does a remarkably good job in fitting synchrotron X-ray data except at low angles where axial divergence effects lead to an asymmetric peak shape [28]. Many empirical corrections have been described in the literature to model this asymmetry; we have had very good success using the more rigorous functional form described by van Laar and Yelon based on the diffraction optics [34].

It is important to remember that the Rietveld method requires an initial structural model. If this is chosen properly then a few refinement cycles are usually sufficient to give a good enough fit that difference Fourier methods can be used to locate any missing atoms. Several Rietveld refinement programs have been developed and are freely available to the user community; widely used ones include GSAS [35], DBW [36], RIETAN [37] and SIMREF [38].

High-resolution synchrotron X-ray powder data are also well suited to the *ab-initio* solution of unknown structures in which the unit cell is first determined by standard auto-indexing techniques and then integrated intensities are obtained by a pattern decomposition process which is analogous

to the Rietveld method but does not involve any structural model. One very convenient procedure for this is described by Le Bail and colleagues [39].

The least-squares fitting procedure involves both structural parameters (e.g. atomic positions, temperature factors and site occupancies) and profile parameters (unit cell parameters, half-width parameters and zero point offset). In the initial stages of a refinement it is often desirable to apply constraints, such as a single temperature factor for all the atoms of the same atomic species, and to relax these as the fit improves. The peak shape parameters tend to be highly correlated, and sometimes physically unrealistic values are obtained (e.g. X or Y may become negative) or the refinement may diverge. With high-resolution synchrotron data it is frequently not possible to refine any of the Gaussian parameters U, V or W. Temperature factors and site occupancies are also highly correlated and this may lead to physically unrealistic results as well; for example a site occupancy should be fixed at unity if it refines to a larger value. Unusually large temperature factors are often indicative of static disorder rather than large thermal fluctuations, or possibly a partially occupied site. It is difficult to determine anisotropic temperature factors reliably from powder diffraction data, and results of this type should be regarded with some caution. If systematic discrepancies of the observed and calculated intensities of a particular class of peaks are noticed, such as the (00ℓ) reflections, for example, preferred orientation should be suspected, especially for flat-plate samples. A generalized correction for this effect requires the use of symmetrized spherical harmonics [40], but this has not yet been incorporated into most of the widely-used programs. Instead, the simple uniaxial March correction [41] is usually applied. The quality of the refinement is assessed by a variety of residual R-factors, based on integrated intensities (R_I, sometimes R_B) or structure factors R_F and R_{F2}, unweighted data points in the diffraction pattern (R_p), weighted data points (R_{wp}) and an expected or statistical residual (R_e), as defined in reference [42]. The ratio $(R_{wp}/R_e)^2$ is the χ^2 weighted-profile goodness-of-fit index, S^2_{wp}.

It is important to recognize that the weights used in the least-squares minimization are usually based solely on counting statistics, which are seldom the limiting source of error in powder diffraction measurements. Thus the estimated errors obtained for the refined parameters (which usually contain the factor S_{wp}) represent a lower limit and may underestimate the "true" errors by a factor 2-3. In addition, R_p and R_{wp} are not in general appropriate for the widely used Hamilton significance tests [43] to assess whether the fit is improved by the inclusion of extra parameters in the structural model. Therefore, what constitutes a significant improvement is largely a matter of subjective judgement. In the case of high resolution synchrotron x-ray data R_p and R_{wp} tend to be dominated by large, predominantly, background regions with very low counting rates, and are not always a good indicator of the fit to the structural model. A better choice is R_I, or perhaps the analogous weighted R-factor R_{wI}, which is not usually quoted but can be calculated easily, and can be be used in the Hamilton significance tests.

From the above discussion, it is clear that if anomalous scattering is used for structural studies, attempts to refine f ' , site occupancies and thermal factors may present problems because of correlations if only a near-edge data set is available. It would then be necessary to fix f ' at some assigned value, based upon either theory or experimental data for a model compound taken

under the same conditions. However, if a second off-edge or neutron data set is simultaneously used in the refinement, the additional constraint on the temperature factors should allow a satisfactory refinement of f' from the near-edge data set. This is the rationale for many of the experiments described in section 3.

As Friedel pairs overlap in a powder diffraction pattern, the amount of useful information about f" that can be extracted from the data is limited. Clearly, in the case of centrosymmetric space groups the situation is much the same as that in the case of single crystal data, but for non-centrosymmetric space groups the lack of access to Bijvoet differences places powder diffraction data at a significant disadvantage when compared to single crystal data. For most practical purposes it is a sufficiently good approximation to fix f" at its theoretical value. However, if the data are of good quality and f" is relatively large, as in experiments at the top of an absorption edge, it is our experience that there is likely to be some sensitivity to f".

Simultaneous refinement can also be used to advantage in the analysis of multiple x-ray data sets collected at several different energies for the same element, or for more than one element. In this context, an interesting strategy has been proposed by Limper et al. [17] namely simultaneous data collection from the primary radiation and its higher harmonics. The use of a neutron data set, collected on the same sample, in such a refinement provides an additional strong constraint on the temperature factors, as previously mentioned, and a much better probe of light elements, of course.

3. EXAMPLES

3.1. Elemental contrast

One of the first powder diffraction studies at a synchrotron to exploit anomalous scattering was the determination of the dopant distribution in substituted $YBa_2Cu_{3-x}M_xO_{7-\delta}$, where M = Fe, Co, Ni and Zn, by Howland and co-workers [44]. These elements are known to have a drastic effect on the superconducting properties of the parent material, and it is clearly important to determine how they are distributed between the Cu(1) "chain" sites and the Cu(2) "plane" sites in the parent structure [45]. Similar materials were previously studied by neutron powder diffraction techniques, but there was some disagreement between the results of different workers, especially for Zn. This is presumably due to the varying contrast between the scattering lengths of Cu ($b = 0.77 \times 10^{-12}$ cm) and the other elements (b = 0.95, 0.25, 1.03 and 0.57 x 10^{-12} cm for Fe, Co, Ni and Zn respectively). Hence, while the problem is well-determined for say, Co, this is not the case for Zn. The x-ray experiments relied on measurements of a few integrated intensities at four energies close to the respective K-edges rather than full Rietveld refinement based on extended data sets. Values of f' were determined experimentally by Kramers-Kronig transformation of absorption data. The variation of the observed intensities was compared with values calculated for different models of the distribution of dopant atoms between the two types of site. The results demonstrated with fair precision that for x = 0.3, Ni and Zn were essentially randomly distributed, while Fe and Co occupied predominantly the chain sites. For Zn substitution a

similar conclusion was reached by Kwei et al. [46] from a Rietveld refinement based on combined neutron and x-ray anomalous scattering data.

An interesting example of neutron and x-ray data used in a simultaneous refinement is the determination of the atom distribution in an alloy of nominal composition $Fe_{0.50}Co_{0.48}V_{0.02}$ by Williams et al. [47]. This alloy has an ordered CsCl-type structure and is an excellent soft ferromagnet of great commercial interest; the small V addition improves the mechanical properties. The Rietveld refinement of the site occupancies employed time-of-flight neutron data and synchrotron x-ray data collected at four different energies. The latter were chosen to be well-above and about 5 eV below the respective Co, Fe and V K-edges. The fraction of each constituent was constrained to the known composition, but the total occupation of each site was not constrained to unity. Theoretical values of f' were employed in this study. The results are summarized in Table 1 and demonstrate the precision that can be attained by this refinement technique.

Table 1
Site occupancies and temperature factors, U, in body-centered cubic $Fe_{0.50}Co_{0.48}V_{0.02}$. Figures in parentheses are estimated standard deviations (esd's) referred to the least significant digit.

	Fe	Co	V	U(Å^2)
Site occupancy at 0,0,0	0.852(3)	0.169(8)	-0.001(7)	0.0042(1)
Site occupancy at 1/2,1/2,1/2	0.148(3)	0.791(8)	0.041(7)	0.0026(2)

Fe and Co are about 85% ordered in the corner and body-centered positions, with V in the latter site. Furthermore, the total occupation of each site is very close to the expected value of unity, which is an additional check of the precision of the results.

Anomalous scattering has been employed by Kumar and colleagues to determine the atom distribution in ordered ternary alloys $Cu(Au_xM_{1-x})$, with M = Ni and Pd [48]. In the prototype tetragonal CuAu-I type of structure, Cu and Au are ordered on the corner and body-centered sites. Extended data sets were obtained close to the Cu, Ni and Pd K-edges and the Au L_{III}-edge, and corrections to the theoretical anomalous terms were made based on measured absorption data. The results from a simultaneous refinement demonstrated that for x = 0.12, Ni preferentially substitutes on the Cu site, while for x = 0.2 and 0.5, Pd substitutes on the Au site. As in the previous example, the fraction of each element was constrained to the known composition, and the total occupation obtained for each site was very close to unity.

In the course of these refinements, it was found necessary to apply a correction for surface roughness, since unphysical, sometimes negative, values were obtained for the temperature factors. This point was investigated

in more detail in subsequent measurements by Sparks et al. [31] in which the Ni Kα fluorescence intensity was monitored as a function of 2θ for several samples as illustrated in Figure 5. The decrease in intensity with decreasing 2θ qualitatively resembles the effect that would be produced by a negative thermal factor, and the authors recommend the incorporation of an extra parameter in the refinement program to allow for situations where such effects might occur, for example, in the case of coarse and highly absorbing powders. Possible corrections of this type have been proposed by Suortti [49] and Hermann and Ermrich [50].

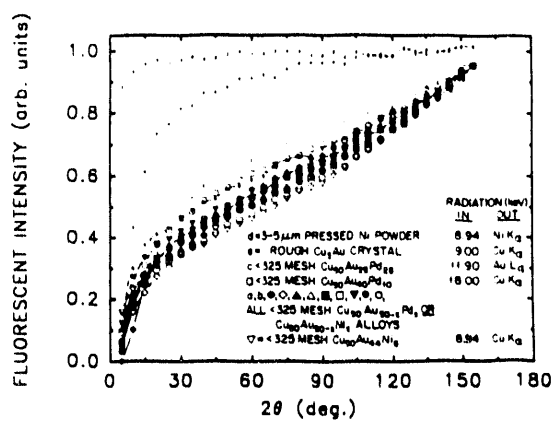

Figure 5. Fluorescence signal from various alloy samples as a function of scattering angle illustrating the effect of microabsorption. In the absence of granularity effects the intensity would be constant. Reproduced from ref. [31] by permission of the authors.

The application of anomalous scattering to a much more complicated crystallograhic problem was recently reported by Perkins and Attfield [51], namely an investigation of the cation distribution in $FeNi_2BO_5$, which has an orthorhombic unit cell with 16 variable positional parameters and four inequivalent metal sites. An energy of 7104 eV was chosen for data collection, which is sufficiently far below the Fe K-edge (7120 eV for Fe_2O_3) to avoid possible difficulties associated with absorption and fluorescence, and any variation of f ' due to chemical environment. Since the Fe atoms in $FeNi_2BO_5$ are in a similar octahedral environment and oxidation state to those in Fe_2O_3, data from the latter, collected under identical conditions, were used to obtain a value of f ' (-6.9 eu) for subsequent use in the refinement of the $FeNi_2BO_5$ structure. This strategy avoids the need to know exactly how far the incident beam energy is from the absorption edge, and in the case of measurements very close to the edge, would take into account the variation of f ' with chemical environment. With the composition fixed at the ideal stoichiometry and the total occupation of each site constrained to unity, the refinement converged satisfactorily, yielding a significantly non-random cation distribution very similar to that previously reported for isostructural $AlNi_2BO_5$ [52].

A comparative study of the elemental contrast obtained with anomalous scattering of x-rays and the traditional neutron technique has been reported by Warner and coworkers [53]. The compounds chosen for study were $Co_2Fe(PO_4)_2$, for which neutrons provide excellent contrast between Fe and Co, with respective scattering lengths of 0.95 and 0.25 x 10^{-12} cm, and the structurally related material $Fe_3(PO_4)_2$, which served as a model compound for the determination of f ' . As in the previous example, only a single data set was collected, at an energy of 7111 eV, about 9 eV below the Fe K-edge determined from XANES data (7119.5 and 7119.8 eV for the Fe and Co compounds, respectively). High resolution time-of-flight neutron data were also taken on the Co compound.

The structure of $Fe_3(PO_4)_2$ is quite complicated, with a monoclinic unit cell, a total of 39 variable positional parameters and three inequivalent metal sites, one six- and two five-coordinated. To allow for possible differences in f ' for the two types of coordination, separate values were refined initially but no significant differences were found, and an average value was assigned in the final stages of the analysis. The refined value of -7.8 eu (which is slightly lower than the theoretical figure of -8.2 eu) was used in the refinement of the $Co_2Fe(PO_4)_2$ structure. This has a smaller monoclinic unit cell, 18 variable positional parameters and two crystallographically distinct metal positions, a five-coordinated fourfold site and a six-coordinated twofold site. The results of independent refinements carried out with the neutron and x-ray data, with the stoichiometric composition assumed and the total occupancy of each site constrained to unity, yielded the results summarized in Table 2.

Table 2
Site occupancies in $Co_2Fe(PO_4)_2$ determined from independent neutron and x-ray refinements [53]. Space group $P2_1/n$, a = 7.5880, b = 8.4246, c = 5.0808 Å, β = 94.093°. Figures in parentheses are estimated standard deviations (esd's) referred to the least significant digit(s).

Site	Coordination	Atom	Occupancy (neutrons)	Occupancy (X-rays)
M(1) 4(e)	5	Fe	0.251(4)	0.243(5)
at x,y,z		Co	0.749(4)	0.757(5)
M(2) 2(c)	6	Fe	0.498(8)	0.514(10)
at 0,0,1/2		Co	0.502(8)	0.486(10)

The results are seen to be in excellent agreement, and even though the x-ray refinement is based on a single data set, the precision is only slightly inferior to that of the neutron refinement.

A further example of the potential of anomalous scattering is provided by some diffraction patterns recently obtained by Nelmes et al. from InSb in a diamond-anvil cell at a pressure of about 3.5 GPa [54]. The diffraction profile derived by integration of the data recorded on an imaging-plate area-detector at an energy of about 25.8 keV is reproduced in Figure 6. The inset shows the enhancement of the low-angle reflection at an energy of 27.886 keV (about 11 eV below the In K-edge) due to the increased contrast between In and Sb, which furnishes crucial information about the phase transformations which occur with increasing pressure in this material.

3.2. Static disorder problems

When two atomic species are distributed over the same set of sites, for example, in a solid solution, it is normally impossible to refine independent

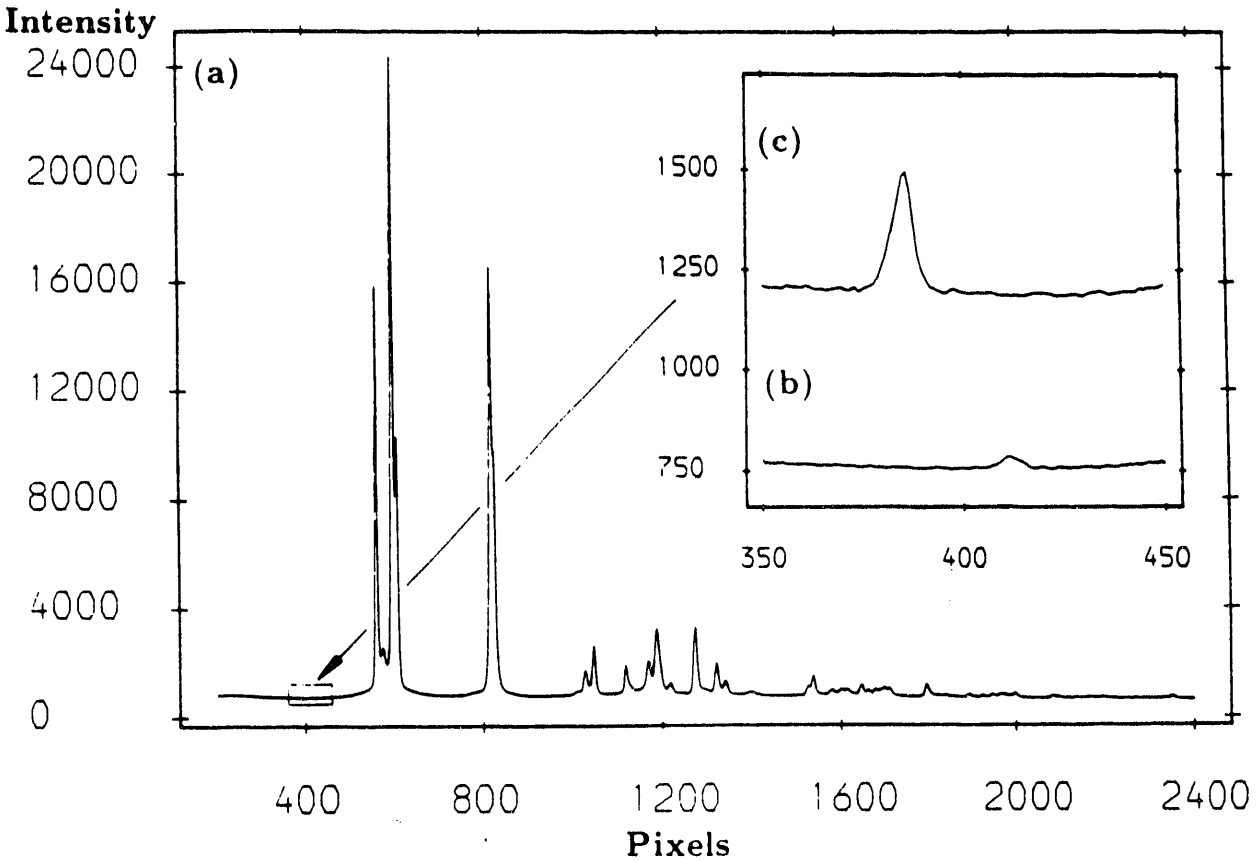

Figure 6. Diffraction pattern from InSb at a pressure of ~ 3.5 GPa recorded on an imaging plate at an x-ray energy of about 11 eV below the In K-edge. The inset shows (b) the enhancement of the difference peak compared with (c) data collected off-edge. Reproduced from ref. [54] by permission of the authors.

temperature factors or coordinates for the species as they are highly correlated. However, it is possible to employ multiple data sets collected at different contrast levels to determine individual temperature factors or coordinates for them. The use of anomalous scattering in this type of problem was demonstrated by Moroney et al. by measurements on an yttria-stabalized zirconia sample with the composition $Zr_{0.81}Y_{0.19}O_{1.90}$ [8]. This material has a defect fluorite-type structure in which a single set of sites is occupied by both Zr and Y, and charge balance is preserved by the formation of vacancies in the oxygen lattice. Crystallographic evidence indicates that there are substantial static displacements of both anions and cations from the usual fluorite positions. From an EXAFS study it was concluded that the Zr cations showed greater displacements than the Y cations [55]. Three sets of synchrotron X-ray powder diffraction data were collected; an off-edge set at 16047 eV, one at 17023 eV (19 eV below the K-edge of Y), and a further one at 17989 eV (10 eV below the

K-edge of Zr). Appropriate values of f ' for Zr^{IV} and Y^{III} were derived from published experimental values for Zr [12] shifted by 3 eV and 961 eV respectively. Refinement based on integrated intensities yielded the mean-square displacements listed in Table 3.

Table 3
Mean square displacements in $Zr_{0.81}Y_{0.19}O_{1.91}$ [8]. Corresponding values for Zr and O in ZrO_2 are 0.011Å^2 and 0.012Å^2 respectively, and 0.009Å^2 for Y in Y_2O_3.

Atom	U(Å^2) (Zr and Y independent)	U(Å^2) (Zr and Y the same)
Zr	0.045(2)	0.041(1)
Y	0.024(6)	
O	0.098(2)	0.098(2)
R_{wF2}	0.018	0.021

Also shown in Table 3 are the results of a refinement with the temperature factors of Zr and Y constrained to be the same. Application of the Hamilton significance test [43] shows that the improved fit with the unconstrained model is highly significant (99.5% confidence level). The results show not only that substantial static disorder is present, but also that Zr is displaced significantly more than Y, consistent with the EXAFS study.

3.3. Site selective measurements

Anomalous scattering is capable of providing information similar to that provided by x-ray absorption measurements, but with the additional advantage that it is crystallographically site-selective. This arises because of the close connection between absorption and the anomalous scattering corrections, which can be determined independently for each site. Such site-specific determinations of the anomalous scattering corrections in the near-edge region can be used to contrast oxidation states in mixed-valence materials and to characterize the coordination geometry around an element at a specific site, even in solid solutions. This approach has already been exploited in several cases, as described in the next two sections; and was very recently extended into the EXAFS region in a quantitative fashion for the study of thin films, multilayers and powders (see the article by Sorensen and coworkers in this book [56]).

3.3.1. Oxidation state contrast

The determination of the distribution of valence states in compounds containing two different oxidation states relies upon the rapid change in f ' close to the absorption edge, which typically shifts to higher energies by a few eV per oxidation state unit. Thus in this region f ' will vary significantly between the differing oxidation states. Measurements of this type have been

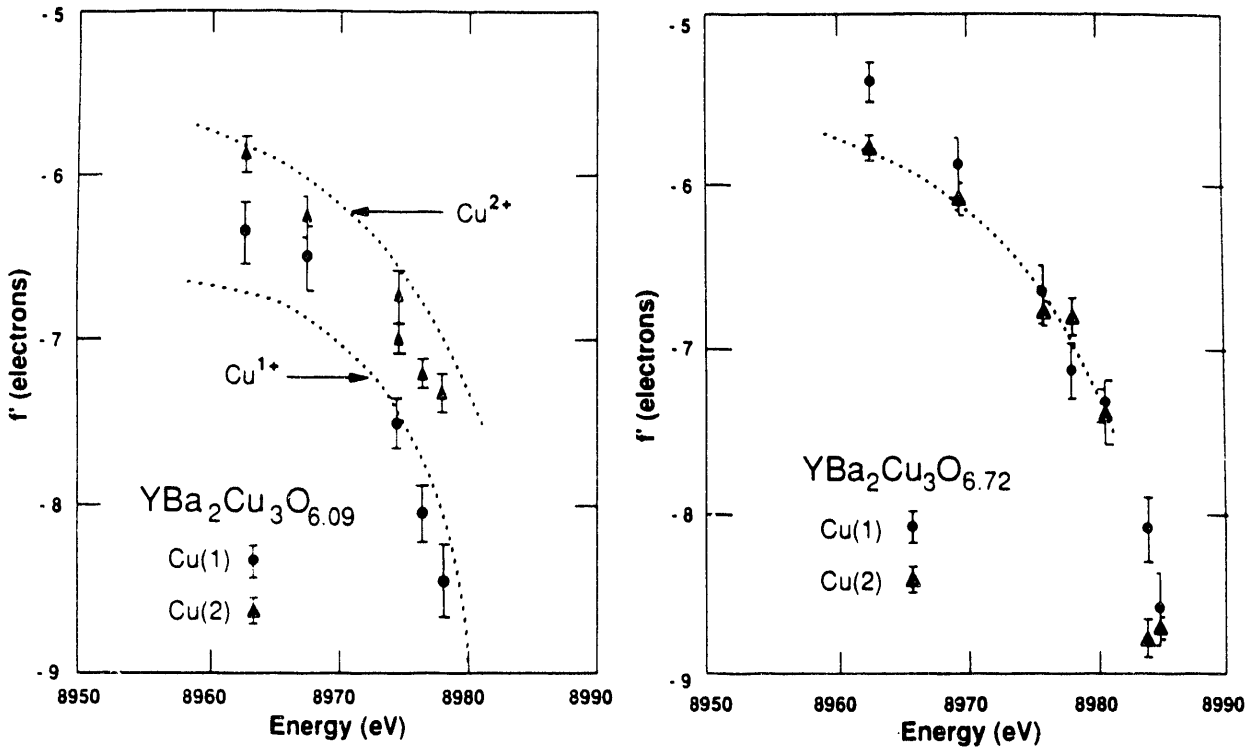

Figure 7. f ' in the vicinity of the K-edge for Cu in the chain, Cu(1) and plane Cu(2) sites in (left) non-superconducting $YBa_2Cu_3O_{6.09}$. The dotted lines show f ' for Cu^I and Cu^{II} in the model compounds Cu_2O and CuO (right) superconducting $YBa_2Cu_3O_{6.72}$. The dotted line shows f ' for Cu^{II}. Reproduced from ref. [46] by permission of the authors.

performed by Kwei and coworkers to probe the oxidation state of Cu in the high T_c superconductor $YBa_2Cu_3O_{6.77}$ and reduced non-superconducting material $YBa_2Cu_3O_{6.09}$ [46]. Initially, combined neutron and synchrotron x-ray data were used to refine f ' as a function of energy near the K-edge for the model compounds Cu_2O, CuO and $KCuO_2$, in which Cu is formally in Cu^I, Cu^{II} and Cu^{III} oxidation states. Neutron and x-ray data were then used to refine values of f ' for the Cu(1) chain and Cu(2) plane sites at several different energies within about 25 eV of the edge. The results are illustrated in Figure 7, and show that in the reduced compound the Cu(1) and Cu(2) sites are occupied by Cu^I and Cu^{II} respectively by comparison with the results obtained for the model compounds shown by the dotted curves. However, no such distinction can be seen for $YBa_2Cu_3O_{6.72}$, nor for two other compositions with oxygen contents of 6.38 and 6.92.

A different approach was adopted by Attfield [57] to probe the oxidation state distribution in $YBa_2Cu_3O_{6.27}$. He derived site-resolved absorption spectra from a combination of fluorescence and diffraction data collected with the same experimental geometry at 12 energies between 8960-9080 eV, i.e. from about 30 eV below to 90 eV above the Cu K-edge. This method requires a knowledge of the instrumental scaling constant and the phases of the structure factors of at least two suitable peaks, in this case (001) and (111), which were determined from an off-edge data set. The absorption spectra were then derived from the

intensities of the fluorescence data following Suortti [58]. The results are reproduced in Figure 8 for the two Cu sites. In spite of the relatively poor resolution due to limitations in the amount of data and the counting statistics, the spectra reveal that the Cu(1) edge is broader with unresolved pre-edge features, and several eV lower in energy than the Cu(2) edge, consistent with XANES results and the generally-held view that both Cu^{I} and Cu^{II} are present on the Cu(1) sites, but only Cu^{II} on the Cu(2) sites [59,60].

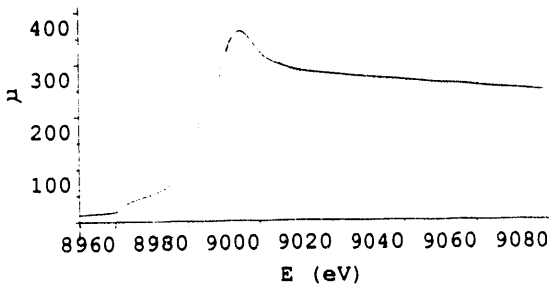

Figure 8. Site-resolved Cu K-edge absorption spectra for the Cu(1) (solid line) and Cu(2) (dashed line) in $YBa_2Cu_3O_{6.27}$ derived as described in text. Reproduced from ref. [57] by permission of the author.

Attfield has also used anomalous scattering in an investigation of the oxidation states and cation distribution in Eu_3O_4 and $EuSm_2O_4$, which have orthorhombic structures with three inequivalent rare-earth metal sites [61]. The results obtained from a refinement of f ' and f " for each of the three sites in Eu_3O_4 demonstrated that Eu^{III} was present on both the M(1) and M(2) sites, and Eu^{II} was found only at the M(3) site, in agreement with previous conclusions based on coordination geometry and other cation substitutions. Based on the experimentally determined values of f ' and f " for Eu and the theoretical values for Sm, it was possible to demonstrate in an analysis of the structure of $EuSm_2O_4$, that the cations were fully ordered with Sm in the M(1) and M(2) positions and Eu^{II} in the M(3) sites.

A detailed study has been reported by Wilkinson et al. [62] of the anomalous scattering in $GaCl_2$, which is a textbook example of a mixed-valence compound, i.e. $Ga^{I}Ga^{III}Cl_4$ [63]. This is a very reactive compound, immediately hydrolyzed by moist air, necessitating the use of sealed capillaries for the diffraction experiments. A channel-cut Si(111) monochromator was used with an energy resolution of about 2 eV. Data were collected at several energies with various diffraction geometries, including the use of two different analyzer crystals and a receiving-slit. The latter was found to give the best compromise between intensity, resolution and reproducibility. The strategy chosen for the data analysis was to refine a structural model for each of the extended data sets with a variable f ' for each of the Ga sites and f " fixed according to the experimental values reported for GaAs [64], since attempts to refine f ' were unsuccessful. Several limited data sets, consisting of scans over a few individual peaks, were also used in separate refinements, but with f' constrained to be the same for both sites. The results are summarized in Table 4 and illustrated in Figure 9.

The most striking feature is that whereas f ' is essentially identical for the Ga^{I} and Ga^{III} sites at lower energies, there is a highly significant difference between the refined values within a few eV of the Ga K-edge at 10370 eV. Based on the experimental values observed for Ga in GaAs [64], the differences in f ' could be interpreted as a shift of about 8 eV from the Ga^{I} to the Ga^{III} edge. However, there is a considerable difference between the minimum value of f ' for $GaCl_2$ and GaAs, namely -12.9 and -10.6 eu, which deserves further

Table 4
Refined values of f ' for Ga in $GaCl_2$ [62].

Energy (keV)	f ' (average)	f ' (Ga^{I})	f ' (Ga^{III})
9932.6		-3.4(1)	-3.3(1)
9933.9	-3.8(3)		
9937.3		-3.9(2)	-3.8(2)
10143.8	-4.1(3)		
10312.4	-5.8(2)		
10352.8		-7.5(1)	-7.1(1)
10353.2		-7.2(1)	-7.2(1)
10354.6	-8.9(2)		
10359.8	-8.3(1)		
10363.3		-10.5(1)	-8.8(1)
10365.5		-10.6(2)	-8.7(3)
10369.5		-12.9(1)	-9.7(2)

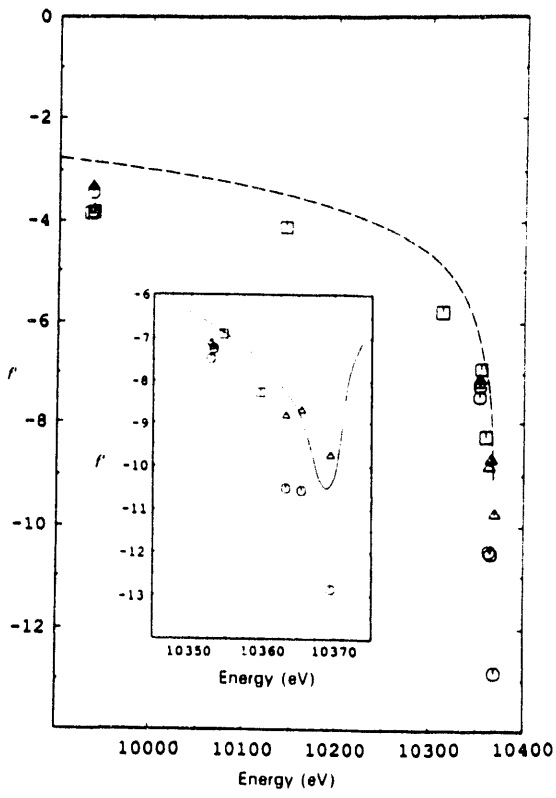

Figure 9. f ' in the vicinity of the Ga K-edge for Ga in $GaCl_2$. The circles and squares are individually refined values for Ga^{I} and Ga^{III} respectively, the squares are average values for f ' constrained to be the same on each site. The dashed line is the theoretical Cromer-Liberman curve with the Ga K-edge shifted to 10370 eV, and the solid line in the inset is the curve obtained by Fukamachi et al. for GaAs [64]. Reproduced from ref. [62].

consideration. X-ray absorption spectra were therefore measured, with a similar bandpass to that used in the diffraction measurements (about 2 eV), for $GaCl_2$ and two model compounds, $GaAlCl_4$ and $GaCl_3$, which contain Ga^{I} and Ga^{III} respectively [65]. As can be seen in Figure 10, the spectra for the latter two compounds show strong white-line features displaced by about 3 eV from each other. A splitting corresponding to these features is seen in the $GaCl_2$ spectrum with the more strongly absorbing component at lower energy, as seen in the data from the model compounds. It is the presence of these strong white-line features which distinguishes $GaCl_2$ from GaAs and prevents a direct comparison of the f ' curves.

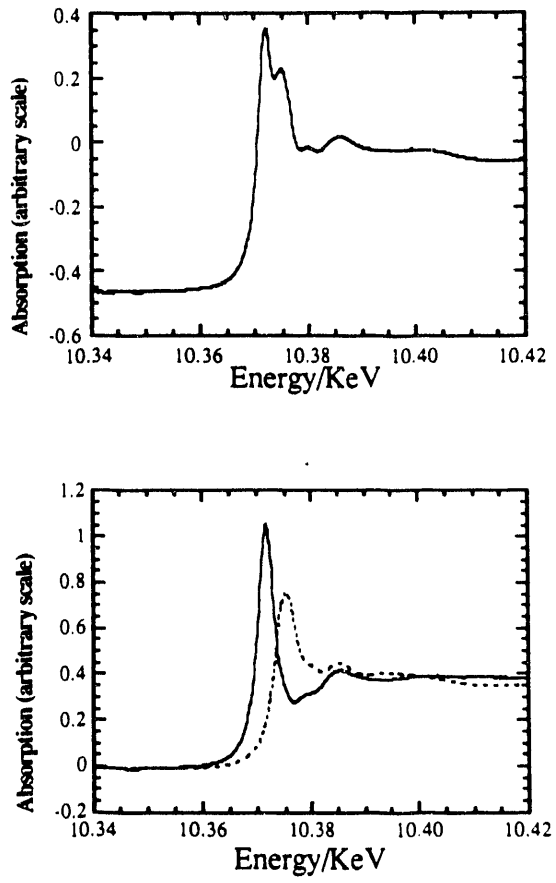

Figure 10. X-ray absorption data for (top) $GaCl_2$ and (bottom) model compounds $GaAlCl_4$ (solid line) and $GaCl_3$ (dashed line), which contain Ga^{I} and Ga^{III} respectively. Reproduced from ref. [65].

Oxidation-state contrast has also been studied in α-Fe_2PO_5, which has an orthorhombic unit cell with 13 variable positional parameters [66]. There are two sets of inequivalent sites for the Fe cations, and Mossbauer spectra indicate ordering of Fe^{II} and Fe^{III} in these sites. XANES data showed a well-defined edge at 7120.9 eV, which was assigned to Fe^{II}, and a less well defined edge for Fe^{III} estimated to be at 7123 eV. Three sets of synchrotron x-ray data collected at 6953, 7118 and 7125 eV were used to refine the structural model, with temperature factors fixed at the values obtained in an independent refinement based on time-of-flight neutron data. Separate values of f ' were refined for each site. The high precision of the refinement is illustrated by the results summarized in Table 5. Identical values were obtained at the lowest energy, but close to the edge a significant difference was found, consistent with the presence of Fe^{II} and Fe^{III} in the Fe(1) and Fe(2) sites respectively.

3.3.2. Site coordination geometry effects

The examples in the previous section demonstrate that significant differences in f ' values for an element in two different oxidation states can be measured in powder diffraction experiments carried out within a few eV of the respective absorption edges. One would also expect differences in f ' for an element in a single oxidation state but with markedly dissimilar coordination geometry.

Table 5
Refined values of f ' for Fe in α-Fe_2PO_5 [66]

Site	f ' (6953.1 eV)	f ' (7118.3 eV)	f ' (7124.8 eV)
Fe(1)	-3.57(4)	-9.74(5)	-6.75(11)
Fe(2)	-3.56(5)	-8.04(7)	-10.01(17)

This has been explored by measurements on the garnet-type compound $Y_3Ga_5O_{12}$, in which Ga occupies both tetrahedral and octahedral sites [25]. Extended data sets were collected at 15442 eV, well above the measured Ga K-edge, and at seven other energies in the range 10318-10390 eV. A refinement of the structure, in which there are three variable oxygen parameters, was carried out for each data set. To reduce correlations, the individual temperature factors for the various atoms were constrained to the values obtained from the off-edge refinement and an overall temperature factor was refined in the other cases. Close to the edge, differences between the f ' values found for Ga in the two types of site varied between -1 and +3.5 eu, as shown in Figure 11.

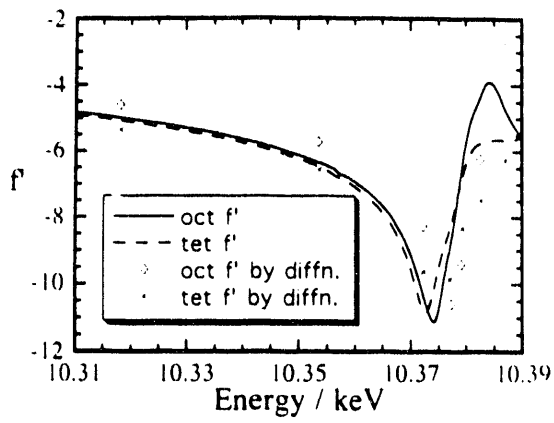

Figure 11. f ' in the vicinity of the Ga K-edge for Ga in $Y_3Ga_5O_{12}$. Squares and crosses are diffraction values for the octahedral and tetrahedral sites respectively. Solid and dashed lines are f ' derived from a Kramers-Kronig transformation of absorption data for model compounds $ZnGa_2O_4$ (octahedral Ga) and $Sr_3Ga_2O_6$ (tetrahedral Ga) respectively [25].

Figure 11 also shows the variation of f ' with energy obtained from a Kramers-Kronig transformation of Ga K-edge absorption spectra measured for two model compounds, $Sr_3Ga_2O_6$ and $ZnGa_2O_4$, which contain Ga in tetrahedral and octahedral sites respectively, as indicated by the broken and solid lines. The latter show that there are indeed significant differences in f ' of up to 2 eu for the two sites, qualitatively in agreement with the diffraction results near the edge if the energy scale is shifted slightly. Such a shift might arise from small errors in calibration, or possibly because the model compounds are not truly representative of the Ga in the garnet. This latter point may also be responsible for the discrepancy between the absolute values of f ' determined from the diffraction data and those from the reference compounds. However, the errors in the values obtained from the Kramers-Kronig transformation may be quite

large and are difficult to quantify. The effects mentioned above would not account for the difference of roughly 0.5 eu between the two sites as determined from the diffraction data, at the lower energies (and also for the off-edge data). This presumably arises from deficiencies in the structural model, such as incorrect temperature factors or perhaps inadequacies in the form factors employed. Additional work is needed to resolve these points.

3.4. Structure solution

While, as mentioned earlier, anomalous scattering diffraction is a widely-used tool in structural macromolecular biology, it has received little attention from the small-molecule and solid-state community. This is undoubtedly a consequence of the rapid advances in conventional structure solution techniques for single crystals of such materials. However, the development of techniques for the solution of structures, in an *ab-initio* fashion, from powder diffraction data is still at a relatively early stage (see, for example, the review by Cheetham and Wilkinson [67] and some very recent work on FIPS (Fast Iterative Patterson Squaring) [68]) and specialized direct methods [69,70]. Only recently has the possibility of solving structures from powder diffraction data using anomalous scattering started to be explored.

Prandl [16] has demonstrated theoretically that such data can be used to solve structures of both centrosymmetric and non-centrosymmetric triclinic phases. In the former case a single type of anomalous scatterer and data at two wavelengths are sufficient, but in the latter case at least two types of anomalous scatterer and data at three wavelengths are needed. His approach was based upon the location of the anomalously scattering atom or atoms using difference Patterson maps followed by the phasing of the data using the intensity ratios of the Bragg reflections at different wavelengths. A practical test of the phasing method of Prandl has recently been successfully performed for the material $CuSO_4 . 5H_2O$. A full discussion of this is given in the article by Limper and Prandl in this book [18].

3.5. Measurements of f'

Although there are several available methods that can be used for the determination of f', as mentioned in section 1, suitable samples are not always available, whereas simple model compounds can be prepared in polycrystalline form for practically every element. The powder diffraction method has the added advantage that f' can, in principle, be determined as a function of 2θ. It is even possible to determine f' for some elements with good accuracy from absolute measurements, as demonstrated by Suortti et al. for Ni powder [9]. However, such measurements require careful experimental technique and data analysis, together with very well-characterized samples. A much simpler technique is to use a simple compound in which the other constituents serve as an "internal standard" for the instrumental scale factor. This method was employed by Will et al. [10] to measure f' for Yb in Yb_2O_3, which has a simple body-centered cubic structure with four variable positional parameters. Data were collected at four energies 8, 21, 60 and 182 eV below the measured L_{III} edge. Integrated intensities were used in the data analysis which was carried out in an iterative ("block refinement") mode for the positional coordinates, the temperature factors and f' in turn, because of the strong correlations. The refinement gave f' values with high precision (0.2 eu),

but differing by 3-5 eu from the Cromer and Liberman values [5,6]. The reason for this rather large discrepancy is not clear.

For this kind of experiment simple binary oxides are not the ideal choice since the scattering will be dominated by the heavier element. In general it is probably a better strategy to select a ternary oxide with a relatively simple structure (e.g. spinel or perovskite-type), and also to collect one data set well away from the edge as discussed in section 3.1. A neutron data set would be particularly useful in this situation.

4. CONCLUDING REMARKS

In this article we have descibed the rapid progress made in the last three years in the application of anomalous dispersion to powder diffraction studies at synchrotron sources. For studies involving element contrast, this can now be regarded as a more-or-less routine aspect of operations at a dedicated powder diffraction beam-line. On the other hand, investigations of oxidation state or coordination geometry effects require careful experimental technique and are much more demanding; in particular, complementary x-ray absorption data should be collected with similar energy resolution whenever possible.

It is worth remembering that there are a few elements for which laboratory sources can be used quite effectively in anomalous scattering experiments without resorting to unusual target materials and exotic emission lines. For example, the Cu $K\alpha$ and $K\beta$ lines ($K\alpha_1$ = 1.5406Å, $K\alpha_2$ = 1.5444Å, $K\beta_{1,3}$ = 1.3922Å) lie very close to the holmium L_{III} (1.5368Å) and L_{II} (1.3905Å) edges (approximately 20 and 10 eV below the edges) respectively, a feature which has been useful in the phasing of single crystal data from $HoNa(edta).8H_2O$ [71], while the energy of Cu $K\beta$ radiation is about 75 eV below the Cu K-edge, corresponding to an f' value of about -4 eu. For Cr and Co the analogous values are about -5 eu. Characteristic $K\beta$ radiation does not appear to have been exploited much in this way, but has some potential use, and has the added advantage that if a semiconductor detector is used, simultaneous collection of an off-edge $K\alpha$ data set is also possible.

Simultaneous collection of on-and off-edge data sets at a synchrotron source, utilizing higher harmonics from the monochromator, is also an intriguing prospect. As pointed out by Limper et al. [17], the effective use of this technique will require mosaic crystals [72] to enhance the intensity of the harmonics. Such crystals would also be very useful as analyzers; the improved integrated reflectivities and counting rates would more than compensate for the slight degradation in energy and angular resolution compared to perfect crystals.

In conclusion, we predict that the combination of high resolution neutron and multi-wavelength synchrotron X-ray data which exploits anomalous scattering, promises to be an extraordinarily powerful tool for the structural characterization of materials in the future.

5. ACKNOWLEDGEMENTS

We would like to acknowledge helpful discussions with A.K. Cheetham, J.P. Attfield and J.K. Warner. Work at Brookhaven was carried out under contract no. No. DE-AC02-76CH00016, Division of Materials Science, U. S. Department of Energy.

6. REFERENCES

1 L.W. Finger, Reviews in Mineralogy, 20 (1989) 309.
2 C.R.A. Catlow in "Applications of Synchrotron Radiation", Chapter 2, Blackie and Son Ltd, London, 1990.
3 D.E. Cox in "Synchrotron Radiation Crystallography", edited by P. Coppens, Chapter 9, Academic Press, New York, 1992.
4 A.J. Bradley and J. W. Rodgers, Proc. Roy. Soc. A144 (1934) 340.
5 D.T. Cromer and D.A. Liberman, J. Chem. Phys. 53 (1970) 1891.
6 D.T. Cromer and D.A. Liberman, Acta Cryst. A37 (1981) 267.
7 R. Begum, M. Hart, K.R. Lea and D.P. Siddons, Acta Cryst. A42 (1986) 456.
8 L.M. Moroney, P. Thompson and D.E. Cox, J. Appl. Cryst. 21 (1988) 206.
9 P. Suortti, J.M. Hastings and D.E Cox, Acta Cryst. A41 (1985) 413.
10 G. Will, N. Masocchi, M. Hart and W. Parrish, Acta Cryst. A43 (1987) 677.
11 D.H. Templeton in "Handbook on Synchrotron Radiation", Vol. 3., edited by G. S. Brown and D. E. Moncton, Chapter 6, North-Holland, New York, 1991.
12 P. Dreier, P. Rabe, W. Malzfeldt and W Niemann, J. Phys. C 17 (1984) 3123.
13 J.J. Hoyt, D. de Fontaine and W.K. Warburton, J. Appl. Cryst. 17 (1984) 344.
14 U. Bonse and I. Hartmann-Lotsch, Nucl. Instr. Methods 222 (1984) 185.
15 B. Lengeler, Proceedings ICAS.
16 W. Prandl, Acta Cryst. A46 (1990) 988.
17 W. Limper, W. Prandl and T. Wrobleski, Mater. Sci. Forum 79-82 (1991) 221.
18 W. Limper and W. Prandl, Proceedings ICAS.
19 W.A. Hendrickson, Proceedings ICAS.
20 P.H. Fuoss, P Eisenberger, W.K. Warburaton and A. Bienenstock, Phys. Rev. Lett. 46 (1981) 1537.
21 T. Egami, Materials Transactions 31 (1990) 163.
22 R. Hu, T. Egami, A.P. Tsai, A. Inoue and T. Masumoto, Phys. Rev. B 46, (1992), 6105 .
23 E. Matsubara and Y. Waseda, Proceedings ICAS.
24 I.G. Wood, L. Nicholls and G. Brown, J. Appl. Cryst. 19 (1986) 364.

25 A.P. Wilkinson, D. Phil. Thesis, Oxford University (1991).
26 A.P. Wilkinson, D.E. Cox and A.K. Cheetham, J. Phys. Chem. Solids 52 (1991) 1257.
27 J.P. Attfield, in "Accuracy in Powder Diffraction II", National Institute of Standards and Technology, Gaithersburg, Maryland, 1992 (in press).
28 H.P. Klug and L.E. Alexander, "X-ray Diffraction Procedures for Polycrystalline and Amorphous Materials", Wiley , New York, 1974.
29 M.O. Krause and J.H. Oliver, J. Phys. Chem. Ref. Data 8 (1979) 329.
30 D.T. Cromer, J. Appl. Cryst. 16 (1983) 437.
31 C.J. Sparks, R. Kumar, E.D. Specht, P. Zschack and G.E. Ice in "Advances in X-ray Analysis", 35, Plenum, New York (1992) 57.
32 H.M. Rietveld, J. Appl. Cryst. 2 (1969) 2.
33 K. Wertheim, M.A. Butler, K.W. West and D.N.E. Buchanan, Rev. Sci. Instr. 45 (1974) 1369.
34 B. Van Laar and W.B. Yelon, J. Appl. Cryst. 17 (1984) 47.
35 A.C. Larson and R.B. Von Dreele, GSAS - General Structure Analysis System, Tech. Rept. LA-UR-86-748, Los Alamos National Laboratory, 1987.
36 D.B. Wiles and R.A. Young, J. Appl. Cryst. 14 (1981) 149.
37 F. Izumi, H. Asano, H. Murata and N. Watanabe, J. Appl. Cryst. 20 (1987) 411.
38 J.K. Maichle, J. Ihringer and W. Prandl, J. Appl. Cryst. 21 (1988) 22.
39 A. LeBail, H. Duroy and J.L. Fourquet, Mater. Res. Bull. 23 (1988) 447.
40 M. Jarvinen, M. Merisalo, A. Pesonen and O. Inkinen, J. Appl. Cryst. 3 (1970) 313.
41 W.A. Dollase, J. Appl. Cryst. 19 (1986) 267.
42 R.J. Hill and R.X. Fischer, J. Appl. Cryst. 23 (1990) 462.
43 W.C. Hamilton, Acta Cryst. 18 (1965) 502.
44 R.S. Howland, T.H. Geballe, S.S. Laderman, A. Fischer-Colbrie, M. Scott, J.M. Tarascon and P. Barboux, Phys. Rev. B39 (1989) 9017.
45 M.A. Beno, L. Soderholm, D.W. Capone II, D.G. Hinks, J.D. Jorgenson, J.D. Grace, I.K. Shuller, C.U. Segre and K. Zhang, Appl. Phys. Lett. 51 (1987) 57.
46 G.H Kwei, R.B. Von Dreele, A. Williams, J.A. Goldstone, A.C. Lawson II and W.K. Warburton, J. Mol. Structure 223 (1990) 383.
47 A. Williams, G.H. Kwei, A.T. Ortiz, M. Karnowski and W.K. Warburton, J. Mater. Res. 5 (1990), 1197.
48 R. Kumar, C.J. Sparks, T. Shiraishi, E.D. Specht, P. Zschack, G.E. Ice and K. Hisatsune, Mater. Res. Soc. Symp. Proc. 213 (1991) 369.
49 P. Suortti, J. Appl. Cryst. 5 (1972) 325.
50 H. Hermann and M. Ermrich, Acta Cryst. A43 (1987) 401.
51 D.A. Perkins and J.P. Attfield, J. Chem. Soc. Chem. Commun. (1991) 229.
52 J.A. Hriljac, R.D. Brown, A.K. Cheetham and L. Satek, J. Solid State Chem. 84 (1990) 288.

53 J.K. Warner, A.P. Wilkinson, A.K. Cheetham and D.E. Cox, J. Phys. Chem. Solids 52 (1991) 1251.

54 R.J. Nelmes, P.D. Hatton, M.I. McMahon, R.O. Piltz, J. Crain, R.J. Cernik and G. Bushnell-Wye, Rev. Sci. Instr. 63 (1992) 1039.

55 C.R.A. Catlow, A.V. Chadwick, G.N. Greaves and L.M. Moroney, J. Am. Ceram. Soc. 69 (1986) 272.

56 L.B. Sorensen, J.O. Cross, J.J. Rehr, H. Stragier, C.E. Bouldin, J.C. Woicik, I.J. Pickering, M. Sansome, J. Marsh, G.N. George, D.J. Tweet, K. Akimoto, I. Hirosawa, K. Kimura, J. Matsui, J. Mizuki and T. Tatsumi, Proceedings ICAS.

57 J.P. Attfield, J. Phys. Chem. Solids 52 (1991) 1243.

58 P. Suortti, Phys. Stat. Solidi b91 (1979) 657.

59 J.M. Tranquada, S.M. Heald, A.R. Moodenbaugh and Y. Xu, Phys. Rev. B38 (1988) 8893.

60 L. Soderholm and G. Goodman, J. Opt. Soc. Amer. B6 (1989) 483.

61 J.P. Attfield, Nature 343 (1990) 46.

62 A.P. Wilkinson, A.K. Cheetham and D.E. Cox, Acta Cryst. B47 (1991) 155.

63 G. Garton and H.M. Powell, J. Inorg. Nucl. Chem. 4 (1957) 84.

64 T. Fukamachi, S. Hosoya, T. Kawamura and M. Okunuki, Acta Cryst. A33 (1977) 54.

65 A.P. Wilkinson and A.K. Cheetham, J. Appl. Cryst (in press).

66 J.K. Warner, A.K. Cheetham, D.E. Cox and R.B. Von Dreele, J. Amer. Chem. Soc. 114 (1992) 6074.

67 A.K. Cheetham and A.P. Wilkinson, J. Phys. Chem. Solids 52 (1991) 1199.

68 M.A. Easterman, L.B. McCusker and C. Baerlocher, J. Appl. Cryst. 25 (1992), 539.

69 G. Cascarano, L. Favia and C. Giacavazzo, J. Appl. Cryst. 25 (1992) 310.

70 J. Jansen, R. Peschar and H. Schenk, J. Appl. Cryst. 25 (1992) 237.

71 G. Chapius, D.H. Templeton and L.K. Templeton, Acta Cryst. A41 (1985) 274.

72 J.R. Schneider, O.D. Goncalves, A.J. Rollason, U. Bonse, J. Lauer and W. Zulehner, Nucl. Instr. Meth. B29 (1988) 661.

DISCLAIMER

This report was prepared as an account of work sponsored by an agency of the United States Government. Neither the United States Government nor any agency thereof, nor any of their employees, makes any warranty, express or implied, or assumes any legal liability or responsibility for the accuracy, completeness, or usefulness of any information, apparatus, product, or process disclosed, or represents that its use would not infringe privately owned rights. Reference herein to any specific commercial product, process, or service by trade name, trademark, manufacturer, or otherwise does not necessarily constitute or imply its endorsement, recommendation, or favoring by the United States Government or any agency thereof. The views and opinions of authors expressed herein do not necessarily state or reflect those of the United States Government or any agency thereof.

DATE
FILMED
8/26/93